APPLIED SCIENCES AND ENGINEERING

# Normal stress difference–driven particle focusing in nanoparticle colloidal dispersion

**Bookun Kim[1], Sung Sik Lee[2,3], Tae Hyeon Yoo[4], Sunhyung Kim[5], So Youn Kim[6], Soo-Hyung Choi[7], Ju Min Kim[1,8]***

Copyright © 2019 The Authors, some rights reserved; exclusive licensee American Association for the Advancement of Science. No claim to original U.S. Government Works. Distributed under a Creative Commons Attribution NonCommercial License 4.0 (CC BY-NC).

**Colloidal dispersion has elastic properties due to Brownian relaxation process. However, experimental evidence for the elastic properties, characterized with normal stress differences, is elusive in shearing colloidal dispersion, particularly at low Péclet numbers (*Pe* < 1). Here, we report that single micrometer-sized polystyrene (PS) beads, suspended in silica nanoparticle dispersion (8 nm radius; 22%, v/v), laterally migrate and form a tightly focused stream by the normal stress differences, generated in pressure-driven microtube flow at low *Pe*. The nanoparticle dispersion was expected to behave as a Newtonian fluid because of its ultrashort relaxation time (2 μs), but large shear strain experienced by the PS beads causes the notable non-Newtonian behavior. We demonstrate that the unique rheological properties of the nanoparticle dispersion generate the secondary flow in perpendicular to mainstream in a noncircular conduit, and the elastic properties of blood plasma–constituting protein solutions are elucidated by the colloidal dynamics of protein molecules.**

## INTRODUCTION

Colloidal dispersion, a mixture of small particles subject to Brownian motion and their suspending liquid, is ubiquitously found in natural and biological phenomena and also in a wide range of industrially relevant products, such as food, paints, cosmetics, and electronic materials (*1*). Understanding the flow behaviors or rheology of such colloidal dispersions as nanoparticle-laden suspension is a prerequisite to successful material formulation and processing design (*1*). For instance, the rate-dependent shear viscosity, such as shear-thinning or shear-thickening behavior, substantially affects the transportation of the colloidal dispersion through pipes; the maximum flow rate is limited by the occurrence of the shear thickening (*1*–*5*). On the other hand, the colloidal dispersion tends to restore a well-dispersed equilibrium state because of the relaxation process driven by Brownian motion and interparticle forces when the spatial distribution of colloidal particles is dehomogenized by flows, which is the source of its viscoelasticity (*1*). Many extravagant non-Newtonian flow phenomena such as rod climbing, usually found in viscoelastic polymeric materials, can be attributed to the normal stress differences generated in shearing flow (*6*). However, despite vast rheological tests, experimental evidence of such fluid-mechanical behaviors induced by the normal stress differences is still elusive for colloidal dispersions composed of rigid spherical particles, particularly at Brownian motion–dominant low–Péclet number (*Pe*) conditions (*5*).

The lack of particle orientability as well as deformability, in the colloidal dispersion of rigid spheres, leads to normal stress differences too weak to experimentally detect (*5*, *7*). However, the presence of the normal stress differences has been long predicted, even at both dilute particle volume fractions and low *Pe* limits (*2*, *3*). The Péclet number represents the relative ratio of the hydrodynamic shear to thermal forces in a shear flow: $Pe = 6\pi\mu_s\dot{\gamma}a^3/k_BT$, where $\mu_s$, $\dot{\gamma}$, $a$, and $k_BT$ represent solvent viscosity, shear rate, colloidal particle radius, and thermal energy, respectively. In a simple shear flow, the first and second normal stress differences ($N_1$ and $N_2$) are defined as $\tau_{11} - \tau_{22}$ and $\tau_{22} - \tau_{33}$, respectively, which are both zero for a Newtonian fluid, where $\tau_{11}$, $\tau_{22}$, and $\tau_{33}$ denote the normal stresses in the velocity, velocity gradient, and vorticity directions, respectively (*6*). Meanwhile, Ho and Leal (*8*) predicted that a hard sphere laterally migrates, when subject to the pressure-driven channel flow in viscoelastic fluid, by the gradients of $N_1$ and $N_2$, which explains the lateral particle migration observed in polymer solutions (*9*).

Here, we report the presence of unique non-Newtonian phenomena in the pressure-driven microtube flow of nanoparticle colloidal dispersion, which apparently shows Newtonian rheological properties. First, we found that noncolloidal particles are focused along the channel centerline. The distinctive non-Newtonian behavior, of particle focusing in nanoparticle dispersion, is analyzed and found to be caused by the normal stress differences. Furthermore, we scrutinized the lateral particle migration to examine the predictions by the existing colloidal theories: $N_1$ and $N_2$ have positive and negative signs in a shearing colloidal dispersion at low *Pe* (*2*, *3*), respectively. In addition, the relaxation time of the nanoparticle dispersion, one of the essential material properties to characterize its elasticity, was measured by analyzing the particle focusing process, using the theoretical prediction based on a second-order fluid model (*6*). Further, we observed the generation of secondary flow in perpendicular to mainstream, eventually resulting in a single line focusing in a straight square channel, which suggests that $N_2$ plays a substantial role in transporting particles in the nanoparticle dispersion. Last, the non-Newtonian elastic property of blood-constituting protein solutions was analyzed with the lateral particle migration in a microfluidic device to determine the origin of blood plasma viscoelasticity (*10*), as recently reported. The analyses demonstrated that the colloidal dynamics in the plasma-constituting major protein solutions lead to their elastic properties.

## RESULTS

### Particle focusing in nanoparticle colloidal dispersion in a circular microtube

We observed the lateral motion of single noncolloidal polystyrene [PS; radius ($a_{ps}$), 3 μm; volume fraction, 0.01% (v/v)] beads suspended in a

[1]Department of Energy Systems Research, Ajou University, Suwon 16499, Republic of Korea. [2]Institute of Biochemistry, ETH Zurich, Zurich CH-8093, Switzerland. [3]Scientific Center for Optical and Electron Microscopy, ETH Zurich, Zurich CH-8093, Switzerland. [4]Department of Molecular Science and Technology, Ajou University, Suwon 16499, Republic of Korea. [5]Corporate R&D, LG Chem, Gwacheon 13818, Republic of Korea. [6]School of Energy and Chemical Engineering, Ulsan National Institute of Science and Technology (UNIST), Ulsan 44919, Republic of Korea. [7]Department of Chemical Engineering, Hongik University, Seoul 04066, Republic of Korea. [8]Department of Chemical Engineering, Ajou University, Suwon 16499, Republic of Korea.
*Corresponding author. Email: jumin@ajou.ac.kr

Downloaded from http://advances.sciencemag.org/ on July 17, 2019

commercially available nanoparticle dispersion (LUDOX HS-40) flowing through a capillary tube [inner radius ($R$), 12.5 μm], as schematically shown in Fig. 1A. The nanoparticle dispersion (used as received) is composed of electrostatic repulsion–stabilized silica nanoparticles [mean radius ($a$), 8.1 nm; coefficient of variance (CV), 0.14; nominal volume fraction of nanoparticles ($\varphi_p$), 0.22; refer to Materials and Methods for the detailed characterization procedure of the nanoparticle dispersion], dispersed in aqueous solution. We confirmed the well-dispersed state of the nanoparticle dispersion with a peak at $q^{peak}$ = 0.31 $nm^{-1}$ in the small-angle x-ray scattering (SAXS) data, corresponding to an average distance of ≅ 20 nm due to the repulsive interaction between the silica nanoparticles (Fig. 1B). Previous rheological tests demonstrated that the nanoparticle dispersion (LUDOX HS-40) behaves as a Newtonian fluid due to its constant shear viscosity and nondetectable linear viscoelastic properties (*11*). However, from the experiments (Fig. 1C; see also fig. S1), it is readily seen that the dynamics of PS beads in the nanoparticle dispersion are substantially different from those in Newtonian fluid, because the PS beads are tightly focused along the channel centerline. PS beads are gradually focused at a flow rate ($Q$) of 20 μl $hour^{-1}$, while the beads move from an inlet to downstream (Fig. 1C, top). The channel Reynolds number ($Re_c = l\langle u\rangle\rho/\mu$) was very small (≃ 0.03), where $l$, $\langle u\rangle$, ρ, and μ are the characteristic length scale ($l = 2R$ for the current circular tube), average velocity in the cross section in a channel, density, and viscosity of the nanoparticle dispersion, respectively. On the contrary, no lateral particle motion is expected in a Newtonian fluid at zero $Re_c$ because of the so-called time-reversibility condition (*5*) or the equilibrium particle position is determined at the middle between channel centerline (≈0.6$R$) by shear gradient and wall lift forces at finite $Re_c$ (*5*). Therefore, the particle focusing along the channel centerline cannot occur in Newtonian fluid irrespective of $Re_c$. In addition, the particle focusing observed in the nanoparticle dispersion cannot be attributed to shear-induced migration, which may arise from the interaction among the PS beads (*12*), because of the very small volume fraction of the PS beads (0.01%, v/v). The measured shear viscosity of the nanoparticle dispersion was constant as 14.5 mPa·s for shear rates up to $\dot{\gamma}$ = 1000 $s^{-1}$ at 20°C, when measured with a rotational rheometer equipped with cone-and-plate geometry (1°, 60 mm diameter), and the Newtonian behavior in shear viscosity is consistent with a previous study (*11*). We performed additional viscosity measurements using parallel-plate geometry with small gap heights (40 mm diameter; gap heights, 20, 30, 50, and 100 μm) to enhance the maximum accessible shear rate range (*13*), which also shows Newtonian behavior up to $\dot{\gamma}$ = 20,000 $s^{-1}$ ($Pe$ ≅ 0.05) (the relative viscosity difference was less than 5% when measured with the parallel-plate geometry having a gap height of 20 μm, as the shear rate was changed from 100 to 20,000 $s^{-1}$).

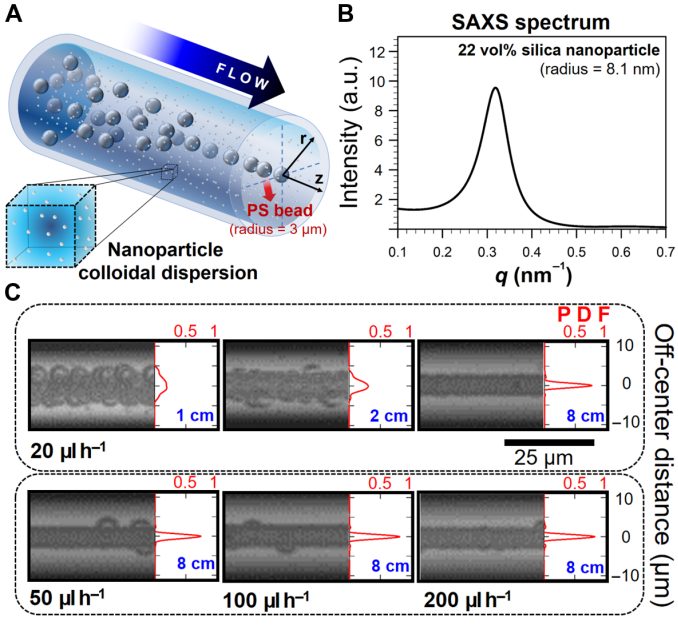


**Fig. 1. Particle focusing in a model nanoparticle dispersion.** (**A**) Schematic diagram for the noncolloidal particle PS bead (6 μm diameter; 0.01 volume %) focusing experiments in a nanoparticle dispersion (nominal volume fraction, 22 volume %; 16.2 nm diameter; LUDOX HS-40) in a circular tube (inner diameter, 25 μm). (**B**) SAXS analysis of the nanoparticle dispersion (LUDOX HS-40). (**C**) Top: Development of particle focusing of the PS beads in a capillary tube at a flow rate of 20 μl $hour^{-1}$ ($Pe_c$ = 0.002). The probability distribution functions (PDFs) were obtained on the basis of the centers of particles, and the labels denote the distance from the inlet. Bottom: Distribution of particles according to flow rates (50 to 200 μl $hour^{-1}$ denoted as labels; 0.005 ≤ $Pe_c$ ≤ 0.02) at a location 8 cm downstream from the inlet. The images were acquired by the $z$ projection of 2000 images using the min intensity mode in ImageJ software (see Materials and Methods for the details of imaging). a.u., arbitrary units.

PS beads form a tightly focused stream up to higher flow rates (200 μl $hour^{-1}$), and the particle focusing is slightly intensified as the flow rate increases (Fig. 1C, bottom). All the experiments presented in Fig. 1C were performed under low–Péclet number conditions (0.002 ≤ $Pe_c$ ≤ 0.02), implying that the spatial distributions of colloidal particles are close to their thermal equilibrium state, where the channel Péclet number $Pe_c$ is defined by $Pe_c = 6\pi\mu_s\dot{\gamma}_c a^3/k_BT$ and $\dot{\gamma}_c$ is the characteristic shear rate $\langle u\rangle/R$. The particle focusing found in the nanoparticle dispersion manifests the non-Newtonian behavior of colloidal dispersion under low–Péclet number conditions not found in colloidal rheology studies (*1*–*5*).

We elucidate that the normal stress differences ($N_1$ and $N_2$) cause the particle migration and focusing in the nanoparticle dispersion. Particle migration, driven by the normal stress differences, was originally proposed to explain the lateral particle motion observed in the pressure-driven flow of viscoelastic polymer solutions (*8*, *9*). Ho and Leal (*8*) predicted with a second-order fluid model that the lateral migration of a rigid spherical particle can be induced by the combined gradients of $N_1$ and $N_2$. In a circular tube, the lateral migration velocity $u_l$ ($r/R$) of a spherical particle, subject to the pressure-driven flow in a second-order fluid, was predicted as the following equation (*14*–*16*)

$$\frac{u_l(r/R)}{\langle u\rangle} = -\alpha Wi\left(1-\beta\frac{N_2}{N_1}\right)\left(\frac{a_{ps}}{R}\right)^2\left(\frac{r}{R}\right) \quad (1)$$

where $Wi$ is the Weissenberg number ( ≡ $\lambda\dot{\gamma}_c$; liquid-like when $Wi \ll 1$, solid-like when $Wi \gg 1$) and λ is the relaxation time of the suspending fluid (*6*). Brunn (*15*) predicted that α and β have positive values of 1.84 and 2.83, respectively. In the equation, the normal stress differences, $N_1$ and $N_2$, were modeled as $N_1/\mu_s\dot{\gamma} = 0.6(1-\varphi_p/\varphi_m)^{-3}Pe$ and $N_2/\mu_s\dot{\gamma} = -0.42(1-\varphi_p/\varphi_m)^{-3}Pe$ ($\varphi_m$; maximum packing fraction), respectively, following previous theoretical models in the low $Pe$ limit for concentrated hard-sphere colloidal dispersions (*3*, *17*) (hence, $N_2/N_1$ is assumed to be −0.42/0.6 in Eq. 1), which may demand further improvement for the repulsive nanoparticle dispersion. However,

Downloaded from http://advances.sciencemag.org/ on July 17, 2019

experimental validation of the predicted $N_1$ and $N_2$ is still challenging, especially at low *Pe*, because of their small magnitudes (*7*). Furthermore, it is not even clear that $N_1$ and $N_2$ have positive and negative signs, respectively, as predicted (*2*, *3*, *17*). However, the positiveness of $N_1$ was observed just before the occurrence of the shear thickening, where *Pe* was non-negligibly large ($Pe \geq 65$) (*18*). In Eq. 1, the combined effects of positive $N_1$ and negative $N_2$ predict the inward particle migration at low *Pe*, akin to the conventional particle migration in viscoelastic polymer solutions with constant shear viscosity (*19*, *20*). Together, the predictions, based on existing colloidal theories (Eq. 1), are consistent with our experimental observations (Fig. 1), supporting the predicted positive and negative signs for $N_1$ and $N_2$ in colloidal dispersion at low *Pe*. However, we note that "particle pressure" (*5*) may play an important role in moving the PS beads suspended in the nanoparticle dispersion at high *Pe*, which was not considered at the current low *Pe* conditions (refer to text S1).

Additional experimental data demonstrated that particle dynamics in the nanoparticle dispersion can be successfully explained with Eq. 1. The particle focusing is intensified with increasing PS bead size or flow rate for a fixed-tube radius, but it is attenuated with decreasing colloidal volume fraction ($\varphi_p$) (refer to fig. S1). Meanwhile, the particle focusing process in the nanoparticle dispersion can be harnessed to characterize its relaxation time similarly as in previous studies on polymer solutions (refer to text S2 and fig. S2 for the detailed procedure and its validation). We observed the radial distribution of the PS beads at each observation location $z_p$ along the streamwise direction and then recorded the outermost radial location ($r_p$) of the PS beads at each $z_p$. The initial position, $r_i$, close to the wall is expected to gradually approach the centerline, and the evolution equation for the PS bead trajectory ($r_p$, $z_p$) can be derived by integrating Eq. 1 as follows (*19*)

$$2\ln\frac{r_p}{r_i}+\left(\frac{r_i}{R}\right)^2-\left(\frac{r_p}{R}\right)^2=-\alpha Wi\left(1-\beta\frac{N_2}{N_1}\right)\left(\frac{a_{ps}}{R}\right)^2\left(\frac{\Delta z}{R}\right) \quad (2)$$

where $\Delta z$ is defined as $z_p - z_i$, and it was assumed that the streamwise velocity of a PS bead is equal to the fully developed Newtonian velocity profile at the PS bead location (*19*, *20*). The outermost location of PS beads ($a_{ps}$ = 1.2 μm; $a_{ps}/R \cong 0.1$) was defined similarly as in our previous work (*19*): the radial location, within which 99% of the particles are distributed near the channel centerline, is defined as $r_p$ at the axial location $z_p$. The left-hand side in Eq. 2, termed the "focusing index" (*19*), and the relaxation time of the nanoparticle dispersion were calculated to be 2.0 ± 0.1 μs (mean ± SD; $n$ = 3) by fitting the focusing index versus $\Delta z/R$ with Eq. 2 for the given flow and geometrical conditions, where $z_i$ is located at 1 cm downstream from the inlet. On the other hand, the relaxation time of colloidal dispersion is defined by the characteristic time required to relax the disturbed colloidal particle distribution to its equilibrium state (*1*, *21*). It was demonstrated that the mean longest relaxation time of colloidal dispersion, which was obtained through the linear viscoelastic properties measured in small amplitude shear flow, is comparable to the characteristic Péclet time scale [$\tau_p \equiv a^2/6D_0^s(\varphi_p)$] for diffusion over a particle radius ($a$) (*21*), where $D_0^s(\varphi_p)$ is the short-time self-diffusion coefficient at colloidal particle volume fraction $\varphi_p$ ($D_0^s(\varphi_p) \rightarrow D_0$ as $\varphi_p \rightarrow 0$). $D_0$ is the free-solution self-diffusion coefficient given by the Stokes-Einstein relation ($D_0 \equiv k_BT/6\pi\mu_s a$). In our experimental condition ($\varphi_p$ = 0.22), $\tau_p$ is predicted to be 0.73 μs according to the theoretical prediction of the short-time diffusion coefficient [$D_0^s(\varphi_p)/D_0 = 1 - 1.832\varphi_p - 0.219\varphi_p^2$] for hard-sphere dispersion (*22*). Our measured relaxation time of 2 μs, determined by analyzing the particle focusing process, does not notably deviate from the estimated diffusion time scale $\tau_p$ = 0.73 μs, which suggests that the main relaxation process in the nanoparticle dispersion originates from the Brownian motion of colloidal particles, as previously observed (*21*).

Until now, the fluid-mechanical phenomena related to the non-Newtonian elastic property at low *Pe* were usually considered to be hard to detect, which can be attributed to the equivalently low-*Wi* condition at low *Pe*. For instance, even the maximum *Wi* is estimated to be only $O(10^{-3})$ in the present experimental conditions due to its ultrashort relaxation time of 2 μs. Therefore, this nanoparticle dispersion can be regarded as having a very small degree of elasticity and behaving similarly to Newtonian fluid. Therefore, the distinctive non-Newtonian phenomenon of the observed particle focusing is apparently counterintuitive, but it is thought to be possible because the trace particles (PS beads) undergo a very large shear strain as estimated to be $\simeq\int\dot{\gamma}dt \approx \dot{\gamma}_c t_{travel} \approx (\langle u\rangle/R)(L/\langle u\rangle) = 6000$ while they travel through the microchannel, where $t_{travel}$ denotes the traveling time of a PS bead through the channel and $L$ corresponds to the channel length.

## Particle focusing in a square channel: Secondary flow effect

We reported that particle focusing in the nanoparticle dispersion is driven by the combined effects of the first and second normal stress differences ($N_1$ and $N_2$), where the magnitudes of the two normal stress differences are quite comparable (*17*). This suggests that $N_2$ plays an important role in migrating the PS beads because $-\beta N_2/N_1$ = 1.98 (*15*, *17*) > 1 in Eqs. 1 and 2. On the contrary, $N_2$ is usually neglected in polymer solutions due to its much smaller magnitude compared with $N_1$ (*20*). We further investigated the $N_2$ effects on the particle focusing and the flow dynamics in a square microchannel, which has non-axisymmetric flow field in the channel cross section. It was demonstrated in polymer solutions that multiple equilibrium particle positions along the centerline and four corners are formed, where the shear rates along these five locations are all zero (consequently $N_1$ = 0) (*23*). This is because the particles are driven toward these positions by the elastic force ($F_e$) exerted on a spherical particle, which is semi-empirically modeled as $F_e \sim -a^3 \nabla N_1$ (*20*). On the other hand, it was numerically predicted that the multiple equilibrium positions in a square channel can be reduced to single-line focusing by the combined effects of the normal stress difference–driven particle migration and the cross-stream secondary flow generated by $N_2$ (*24*). Therefore, we postulated that the nontrivial $N_2$ in the nanoparticle dispersion may change the multiple equilibrium particle positions to a single particle stream within the cross section of a square channel, as schematically drawn in Fig. 2A. We investigated the spatial distribution of the 0.01% (v/v) PS beads ($a_{ps}$ = 3 μm) flowing through a straight, square, poly(dimethylsiloxane) (PDMS) channel [width × height ($w \times h$), 25 μm × 25 μm; length, 5 cm]. As shown in Fig. 2B, single-line focusing is formed along the channel centerline in the nanoparticle dispersion (LUDOX HS-40), which was observed for a range of flow rates (20 to 100 μl hour$^{-1}$) ($0.0008 \leq Pe_c \equiv 6\pi\mu_s\dot{\gamma}_c a^3/k_BT \leq 0.004$; $0.02 \leq Re_c \equiv l\langle u\rangle\rho/\mu \leq 0.1$), where the characteristic length ($l$) and shear rate ($\dot{\gamma}_c$) are defined by $l = 2h$ and $\dot{\gamma}_c \equiv 2\langle u\rangle/h$. The single-line focusing in the square channel supports the generation of the secondary flow. In addition, to more directly validate the secondary flow generation in the nanoparticle dispersion, we investigated dye mixing in a square

Downloaded from http://advances.sciencemag.org/ on July 17, 2019

microchannel ($w \times h$, 25 μm × 25 μm; length, 4 cm), as shown in Fig. 2 (C and D). The same three fluid streams except for the presence of the fluorescent dye flowed into the square channel: A small amount of fluorescent dye [250 parts per million (ppm)] was added to the two side streams and not to the central stream. We observed that the fluorescence intensity profile in the nanoparticle dispersion gradually became homogenized as the fluid streams moved downstream (Fig. 2D), which contrasts with the constant profiles irrespective of the axial location in a Newtonian fluid (Fig. 2C), corroborating the generation of a cross-stream secondary flow. $N_2$ is considered to cause the secondary flow (*25*, *26*) in noncircular tubes, which was also recently found in non-Brownian suspensions (*26*). The secondary flow generation, found in the nanoparticle dispersion, suggests that $N_2$ plays an important role in the flow dynamics of the nanoparticle dispersion and, consequently, affects the transportation of the suspended particles.

## Particle migration in blood plasma–constituting protein solutions

Particle migration and focusing in the model colloidal dispersion (LUDOX HS-40) suggests that non-Newtonian fluid properties may appear in biological colloidal dispersions, such as protein solutions, through the colloidal dynamics. However, electrolytes are abundant in biological fluids, which may substantially change the colloidal dynamics by screening the electrostatic repulsion interaction between colloidal particles (*1*). Colloidal dispersions such as the nanoparticle dispersion, in which the van der Waals attractive force is relevant,

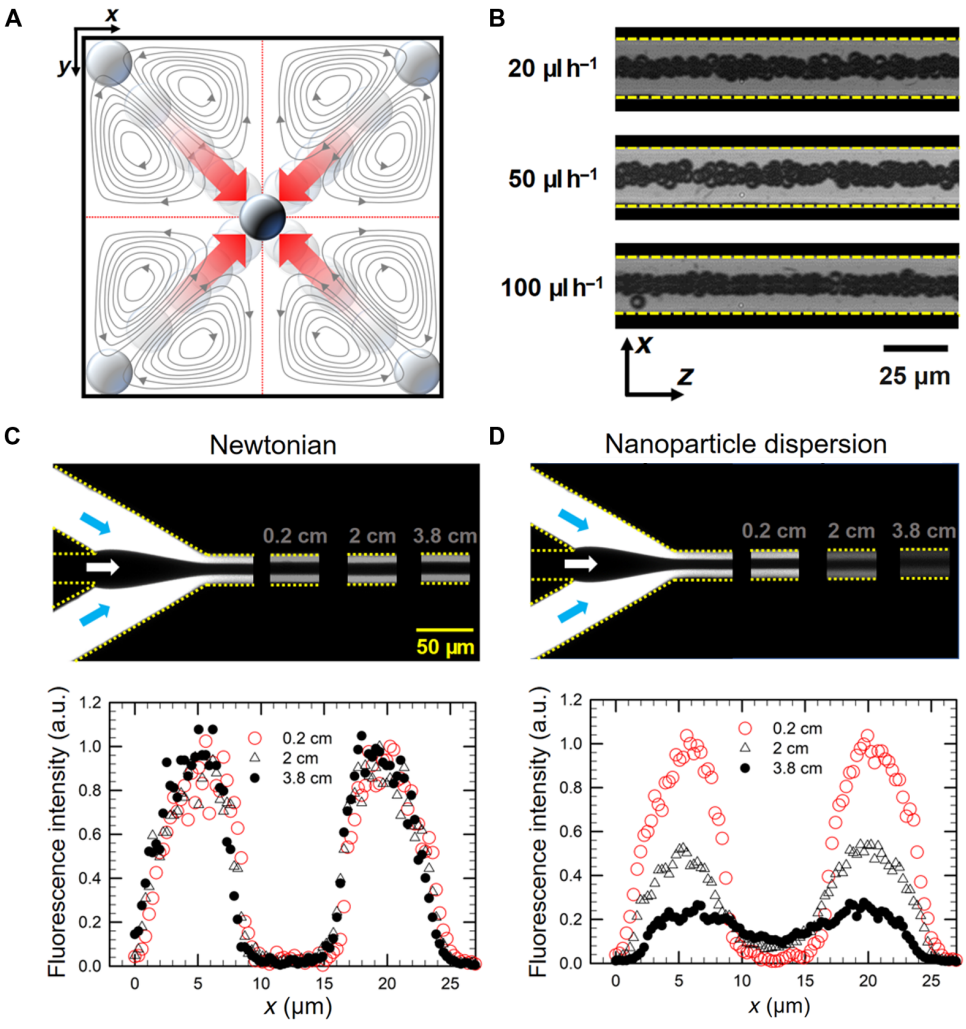


**Fig. 2. Secondary flow generation in a square channel in the nanoparticle dispersion.** (**A**) Schematic diagram for the secondary flow–assisted single-line focusing in a square channel and an overlay of the postulated streamlines for the secondary flow generated by the second normal stress difference ($N_2$). (**B**) Distributions of PS beads in a square straight PDMS channel ($w \times h$, 25 μm × 25 μm; length, 5 cm) for the flow rates ranging from 20 to 100 μl hour$^{-1}$ at a location 4.8 cm downstream from the inlet. The images were acquired by the *z* projection of 2000 images using the min intensity mode in ImageJ software (see Materials and Methods for the details of imaging). (**C** and **D**) Visualization experiments to investigate the mixing occurrence in Newtonian fluid (C) (65 wt % glycerin aqueous solution; viscosity, 15.2 mPa·s) and nanoparticle dispersion (D) (viscosity, 14.5 mPa·s; LUDOX HS-40) in a square channel. The same three fluid streams flowed into a square straight PDMS channel ($w \times h$, 25 μm × 25 μm; length, 4 cm) except for the presence of the fluorescent dye; the fluorescent dye was added to the two side streams and not to the central stream (total flow rate in the straight region: 50 μl hour$^{-1}$). The fluorescence intensity profiles were measured along the cross-stream direction at locations 0.2, 2, and 3.8 cm downstream from the junction point of the three streams.

Downloaded from http://advances.sciencemag.org/ on July 17, 2019

are practically stabilized with electrostatic repulsion and/or steric hindrance, as in the current nanoparticle dispersion (*1*). In a repulsive colloidal dispersion, the contribution of interparticle repulsive forces to the total normal stress differences may dominate over Brownian and hydrodynamic forces between colloidal particles as the ratio of $a_{eff}/a$ increases (*2*, *27*). The effective colloidal radius $a_{eff}$ is introduced to accounts for the interparticle repulsion so that the distance between particles is maintained to be $>2a_{eff}$ (*2*). To understand the effects of the electrostatic repulsion screening on the elastic properties, we investigated particle migration in the nanoparticle dispersion mixed with an electrolyte solution [20× phosphate-buffered saline (PBS) = 19:1; LUDOX HS-40], of which the ionic strength is assumed to be comparable with 1× PBS (ionic strength, 163 mM). As a reference, a slightly diluted dispersion with deionized (DI) water (LUDOX HS-40/DI water, 19:1) was also prepared to match the volume fraction ($\varphi_p = 0.21$; $\varphi_{eff} \equiv (a_{eff}/a)^3 \varphi_p = 0.36$), where $\varphi_{eff}$ denotes an effective volume fraction (see Materials and Methods for how to determine $\varphi_{eff}$). All the experiments in the PBS solution were performed within 1 hour after PBS was added to the original nanoparticle dispersion, because the aggregation of colloidal particles progresses slowly (*28*). The PBS addition substantially reduced the repulsive interactions, as shown in the SAXS and shear viscosity data (Fig. 3, A and B), and consequently, $\varphi_{eff}$ was reduced to 0.25, which is quite close to its nominal volume fraction, $\varphi_p = 0.21$. In the PBS-added solution, we found no discernible particle focusing at a flow rate of either 50 or 100 μl hour$^{-1}$ (Fig. 3, C and D), indicating the weakening of the elastic property by the screening of electrostatic repulsion under the physiological conditions (*2*, *27*).

Fundamental studies on particle focusing in the model colloidal dispersions provide a clue for understanding the origin for the elastic properties of human blood plasma (*10*), as recently observed, which has not yet been well understood mainly due to its very short relaxation time ($10^{-3}$ to $10^{-5}$ s) (*29*). The elastic nature of human blood plasma was identified only in the extensional flows of the capillary breakup extensional rheometer and contraction-expansion geometry, in which the stretching dynamics of the polymer may play a key role in generating viscoelasticity (*10*, *29*). However, the shear flow characteristics are dominant over the extensional flow in blood vessel flow. In addition, the extent of polymer stretching in shear flow is limited because of its rotational component compared to that in the extensional flow (*30*). Therefore, the behaviors of protein molecules as rigid colloidal particles would be more pronounced than the behaviors of flexible polymers in shear flow. Blood plasma is a complicated aquatic mixture composed of diverse inorganic and organic materials including many different protein families such as albumin, globulin, and fibrinogen, where the globulin is again subcategorized into four subclasses: α 1, α 2, β, and γ types (*31*). Here, we focus on two major proteins (albumin and γ-globulin) in blood plasma, where γ-globulin is the richest globulin type (*32*). First, we examined the lateral particle migration in a bovine serum albumin (BSA) solution in the microfluidic device presented in Fig. 4A. Albumin is the most abundant among the proteins that constitute blood plasma. Early studies demonstrated

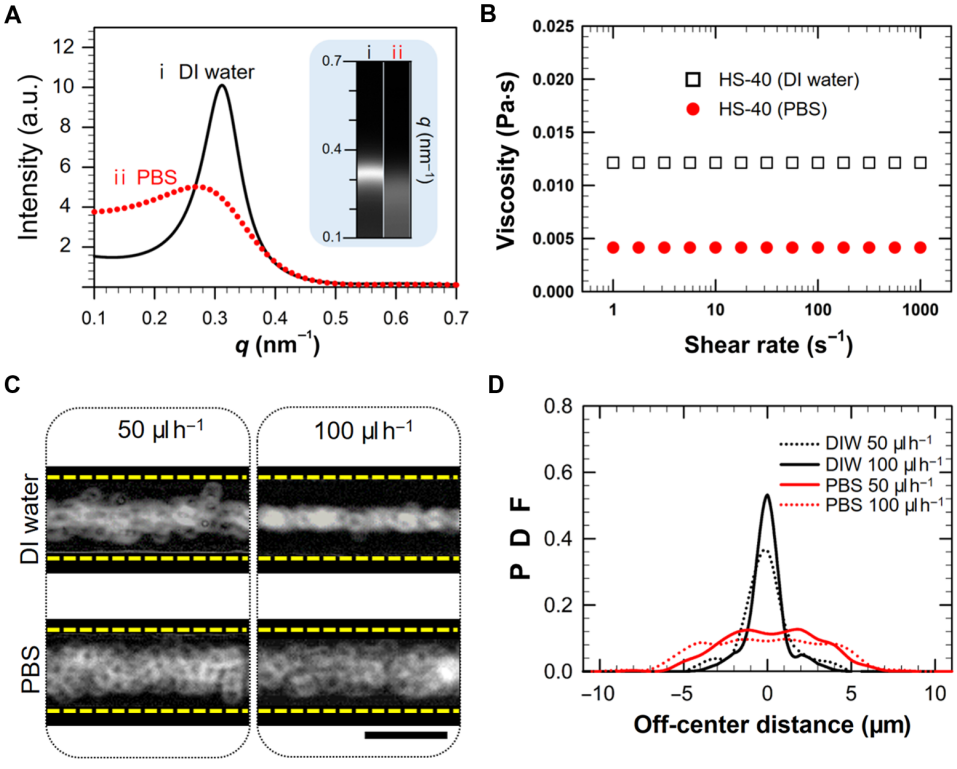


**Fig. 3. Screening effect of the electrostatic repulsive interaction on the elastic property of the model nanoparticle dispersion by electrolyte addition.** (**A**) SAXS analyses of DI water and PBS-added nanoparticle dispersions (final PBS concentration ≈ 1× PBS; $\varphi_p = 0.21$). (**B**) Shear viscosity data in DI water and PBS-added nanoparticle dispersions. (**C**) Particle distributions in DI water and PBS-added nanoparticle dispersions in a square PDMS channel ($w \times h$, 25 μm × 25 μm; length, 5 cm) at a location 4.8 cm downstream from the inlet at flow rates of 50 and 100 μl hour$^{-1}$. The images were acquired by the *z* projection of 2000 images using the standard deviation mode in ImageJ software (see Materials and Methods for the details of imaging). (**D**) PDFs in DI water (DIW) and PBS-added nanoparticle dispersions.

Downloaded from http://advances.sciencemag.org/ on July 17, 2019

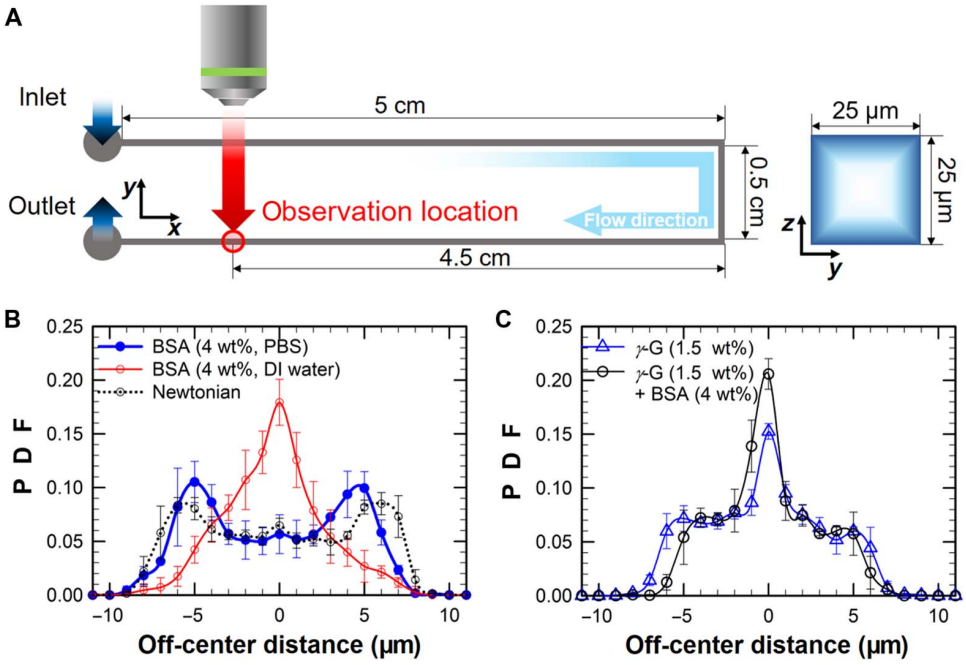


**Fig. 4. Particle focusing in blood plasma–constituting protein solutions.** (**A**) Schematic diagram for the PDMS microchannel used for the lateral particle migration experiments in protein solutions. The data and error bars denote average values and standard deviations, respectively ($n$ = 5). (**B**) PDFs in 4% (w/w) BSA solution in DI water, Newtonian fluid [15% (w/w) glycerin solution in DI water], and 4% (w/w) BSA solution in 1× PBS solution at a flow rate of 10 μl hour$^{-1}$. (**C**) PDFs in 1.5% (w/w) γ-globulin (γ-G) solutions and in a mixture of 1.5% (w/w) γ-globulin and 4% (w/w) BSA in 1× PBS at a flow rate of 10 μl hour$^{-1}$. The data and error bars denote average values and standard deviations, respectively ($n$ = 3).

that the BSA solution behaved like a yield stress fluid, the origin of which was attributed to the lattice structure formed by repulsive interactions among BSA molecules, as found in SAXS experiments (*33*, *34*). However, a more recent study has suspected that the highly non-Newtonian characteristics of the BSA solution, observed in rotational rheometer experiments, may originate from the interfacial viscoelasticity caused by the accumulated proteins at the liquid-air interface (*35*).

Here, PS beads ($a_{ps}$ = 3 μm) were transported through the microfluidic channel depicted in Fig. 4A in DI water and 1× PBS solution at 4% (w/w) BSA concentration, a concentration that is within physiological conditions [reference range, 3.5 to 5.5 g dl$^{-1}$ (*32*)]. We note that there is no liquid-air interface as the solutions are being injected into the microchannel from a syringe. We observed that the PS beads in DI water were noticeably aligned along the channel centerline, while no notable particle focusing was detected in the BSA solution in PBS solution (Fig. 4B). For reference, we also demonstrated the lateral particle distribution in a Newtonian fluid [15% (w/w) glycerin solution in DI water], which also showed no noticeable particle focusing along the channel centerline (Fig. 4B) (refer to text S3). The experimental results indicate the notable elasticity of the BSA solution in DI water, which is substantially reduced in PBS, akin to the experimental observation in the model nanoparticle dispersion. The non-elastic property observed in the PBS solution implies that BSA is not solely responsible for the blood plasma elasticity in the physiological condition, which is seemingly the same conclusion as the previous study (*10*), in which BSA aqueous solution was examined for the blood plasma elasticity (*10*).

Next, we investigated the particle focusing in bovine γ-globulin [reference range, 0.7 to 1.7 g dl$^{-1}$ (*32*)] solutions in PBS solution. The protein γ-globulin is not just one kind of protein but rather is a mixture of immunoglobulins: IgG (80%), IgM (10%), and IgA (<10%) (*36*). The size of the most abundant subclass, IgG, was found to have a radius of gyration ($R_g$) of 5.3 nm (*36*), and the radii of IgM and IgA are larger than or comparable to that of IgG [also compare $R_g$ = 2.8 nm for BSA (*37*)]. As shown in Fig. 4C, the particle focusing is pronounced in 1.5% (w/w) γ-globulin solution in PBS solution. Therefore, experimental results suggest that γ-globulin may play an important role in generating the elasticity of blood plasma. It was recently observed that dimers formed by short-range interactions are abundant in γ-globulin solution (*36*), and monoclonal IgG1 formed "large, loosely bound, transient clusters" in electrolyte solutions (*38*) different from BSA. From the viewpoint of colloidal dynamics, we propose that the elastic properties of the γ-globulin solution originate from (i) the large sizes of γ-globulin molecules or dimers [$N_1$, $N_2 \sim a^3$ (*3*, *17*)], as compared with BSA (*36*, *37*), and (ii) the dynamic network structure formed by the interaction among γ-globulins (*38*). The particle distributions in the γ-globulin solution have shoulders (Fig. 4C), which may be attributed to the formation of dynamic clusters possibly subject to the local shear rate; this demands further study. The particle focusing was further intensified when 4% (w/w) BSA was added to a 1.5% (w/w) γ-globulin solution in PBS (see Fig. 4C). The enhanced elasticity observed in the γ-globulin and BSA mixture suggests the formation of complexes between γ-globulin and BSA molecules, which implies that the elastic properties of blood plasma are affected by complicated protein interactions among different proteins.

## DISCUSSION

This study demonstrated particle (noncolloidal sized) focusing in pressure-driven microscale flow in a nanoparticle dispersion. This phenomenon was elucidated by considering the particle migration

Downloaded from http://advances.sciencemag.org/ on July 17, 2019

induced by the gradients of the normal stress differences. We report that colloidal dynamics, in the model nanoparticle dispersion, drives the very weak elastic property that is represented by an ultrashort relaxation time [O(*1*) μs]. The current results suggest the possible occurrence of size-based particle segregation because of the normal stress differences induced by the colloidal dynamics during material processing, when the material is composed of multisized particles from nano- to micrometer, e.g., lithium-ion battery electrode materials. In addition, we expect that the single-line focusing formation, regardless of the channel cross-sectional shape (Figs. 1 and 2), will find practical use in lab-on-a-chip applications such as particle counting and sorting (*23*). Last, we mention that the blood plasma–constituting proteins are much more diverse than those in the current studies, and the protein species or the protein-protein interaction that have not been investigated in this study may generate stronger viscoelasticity than the current cases. Nonetheless, understanding that blood plasma viscoelasticity can be expressed by the colloidal dynamics of blood plasma–constituting major proteins is an important result. We expect that the studies on the relationship between the composition of the blood plasma–constituting proteins and the viscoelastic properties will open novel routes to understanding the blood cell dynamics, e.g., the lateral cell distribution affected by the elastic property originating from the protein colloidal dynamics that may be affected by human health conditions.

## MATERIALS AND METHODS

### Materials

A commercial nanoparticle dispersion (LUDOX HS-40; Sigma-Aldrich), composed of electrostatic repulsion–stabilized silica nanoparticles (40%, w/w) dispersed in aqueous solution, was used as received, in which the particle volume fraction ($\varphi_p$) and Debye length ($\kappa^{-1}$) were reported to be 0.22 and 1.3 nm, respectively (*11*). The microscopic structure of the nanoparticle dispersion was analyzed with SAXS data (beamline: 4C SAXS II; Pohang Accelerator Laboratory, Korea). The colloidal size in LUDOX HS-40 was measured to be $a$ = 8.1 nm, along with a CV of 0.14, through form factor analysis. The shear viscosity was measured with a commercial rotation rheometer at 20°C [6 cm diameter, cone-and-plate geometry (1°) or 4 cm diameter, parallel-plate geometry; AR-G2, TA Instruments]. Following a previous study (*11*), the electrostatic repulsion among colloidal particles was modeled with an effective radius ($a_{eff}$ = 9.7 nm), slightly larger than the previous estimation (*11*), by mapping the viscosity of the nanoparticle dispersion (μ = 14.5 mPa·s) to a modified hard-sphere viscosity model, $\mu = \mu_s[1 - (\varphi_p/\varphi_m)(a_{eff}/a)^3]^{-2}$, where the maximum packing fraction ($\varphi_m$) was chosen to be 0.51 (*11*). The effective volume fraction [$\varphi_{eff} = \varphi_p(a_{eff}/a)^3$] of LUDOX HS-40 was estimated to be 0.38. PS beads with three different diameters were used as trace particles for the particle focusing and migration experiments: 2.4 μm (CV, 0.05), 4.4 μm (CV, 0.03), and 6 μm (CV, 0.05; Polysciences), and the synthesis procedures for the 2.4- and 4.4-μm PS beads were previously reported (*23*). The sizes of the PS beads were characterized with a Coulter counter (Z2, Beckman). The PS beads were washed three times before their usage with 0.1% (v/v) Tween 20 (Sigma-Aldrich) aqueous solution, followed by a final washing with 1× PBS solution. For the mixing experiment in a square channel, 250 ppm isothiocyanate-dextran [molecular weight ($M_W$), 2000 kg/mol; Sigma-Aldrich] was added to Newtonian fluid [65% (w/w) glycerin (Sigma-Aldrich) aqueous solution; shear viscosity, 15.2 cP at 20°C] or the nanoparticle dispersion (LUDOX HS-40). For the particle migration experiments in protein solutions, BSA (Sigma-Aldrich, product no. A7906) and/or bovine γ-globulin (Sigma-Aldrich, product no. G5009) were prepared by dissolving the proteins in DI water or 1× PBS solution. The shear viscosities of the 4% (w/w) BSA solution in DI water and the Newtonian fluid [15% (w/w) glycerin (Sigma-Aldrich) solution in DI water] were 1.3 and 1.5 mPa·s, respectively [a small amount of nonionic surfactant (Tween 20) was added to the BSA solution for viscosity measurements to preclude the interfacial viscoelasticity (*10*)]. The bovine γ-globulin–including solutions were filtered before the particle migration experiments with a syringe filter.

### Microfluidic setups and imaging

Particle migration experiments were performed in a cylindrical fused silica microtube [inner radius ($R$), 12.5 μm; length, 10 cm; PEEKSil Tubing, catalog no. 62510, Upchurch] or PDMS channels. PDMS channels were fabricated as in our previous study (*39*). For the particle migration experiments, we used almost the same microfluidic setup as in our previous study (*19*) except for slight modifications: The flow rate was controlled with a syringe pump (11 Plus, Harvard Apparatus), and the images were captured with a high-speed camera (MC2, Photron) installed on an inverted optical microscope (IX71; Olympus) equipped with ×20 objective (×1.6 internal magnification was applied), and the acquired images were analyzed with ImageJ software (National Institutes of Health). All the particle locations in both fused silica tube and PDMS channels were analyzed as in the previous study (*19*) except for the 6-μm PS beads in the fused silica tube, which were determined by manually checking the center of each bead with the ImageJ software, because of the low optical contrast ratio of the PS beads near the channel wall. The time-lapse images were stacked in $z$ projection with the "min intensity" or "standard deviation" option in the ImageJ software to qualitatively demonstrate the extent of the particle focusing; the min intensity option was selected to show maximally scattered particle locations near the channel centerline, whereas the standard deviation option was chosen to qualitatively present the average particle distribution (*19*). The contrast and brightness for the dark image, stacked with the min intensity option in ImageJ software, was evenly enhanced. For the mixing visualization experiments in a square PDMS channel, the same three fluid streams were flowed into a square PDMS channel ($w \times h$, 25 μm × 25 μm; length, 4 cm) except for the presence of the fluorescent dye: A small amount of fluorescent dye (250 ppm) was added to the two side streams and not to the central stream. The two side streams emanated from an inlet, and the total flow rate of the two side streams and the central stream flow rate were equally controlled with the two equivalent syringes (500 μl, Hamilton) equipped on a syringe pump (11 Plus, Harvard Apparatus). The images were acquired with a charge-coupled device camera (DMK 23U445) installed on an inverted optical microscope (IX71, Olympus) equipped with ×20 objective. We used the same fluorescence experimental setups and data analysis procedure as in the previous study (*40*).

## SUPPLEMENTARY MATERIALS

Supplementary material for this article is available at http://advances.sciencemag.org/cgi/content/full/5/6/eaav4819/DC1

Supplementary Text S1. Particle pressure–driven lateral migration.

Supplementary Text S2. Measurement of relaxation time using particle migration.

Supplementary Text S3. Inertial particle migration.

Fig. S1. Distributions of PS beads according to flow rates, particle sizes, and colloidal particle volume fractions.

Fig. S2. Measurement of the relaxation time of nanoparticle dispersion (LUDOX HS-40).

References (*41*–*52*)

Downloaded from http://advances.sciencemag.org/ on July 17, 2019

## REFERENCES AND NOTES


1. J. Mewis, N. J. Wagner, *Colloidal Suspension Rheology* (Cambridge Univ. Press, 2012).
2. J. Bergenholtz, J. F. Brady, M. Vicic, The non-Newtonian rheology of dilute colloidal suspensions. *J. Fluid Mech.* **456**, 239–275 (2002).
3. J. F. Brady, M. Vicic, Normal stresses in colloidal dispersions. *J. Rheol.* **39**, 545–566 (1995).
4. D. R. Foss, J. F. Brady, Structure, diffusion and rheology of Brownian suspensions by Stokesian dynamics simulation. *J. Fluid Mech.* **407**, 167–200 (2000).
5. É. Guazzelli, J. F. Morris, *A Physical Introduction to Suspension Dynamics* (Cambridge Univ. Press, 2012).
6. R. B. Bird, R. C. Armstrong, O. Hassager, *Dynamics of Polymeric Liquids* (Wiley Interscience, 1987), vol. 1.
7. R. G. Larson, *The Structure and Rheology of Complex Fluids* (Oxford Univ. Press, 1999).
8. B. P. Ho, L. G. Leal, Migration of rigid spheres in a two-dimensional unidirectional shear flow of a second-order fluid. *J. Fluid Mech.* **76**, 783–799 (1976).
9. A. Karnis, S. G. Mason, H. L. Goldsmith, Axial migration of particles in Poiseuille flow. *Nature* **200**, 159–160 (1963).
10. M. Brust, C. Schaefer, R. Doerr, L. Pan, M. Garcia, P. E. Arratia, C. Wagner, Rheology of human blood plasma: Viscoelastic versus Newtonian behavior. *Phys. Rev. Lett.* **110**, 078305 (2013).
11. E. Di Giuseppe, A. Davaille, E. Mittelstaedt, M. François, Rheological and mechanical properties of silica colloids: From Newtonian liquid to brittle behaviour. *Rheol. Acta* **51**, 451–465 (2012).
12. D. Leighton, A. Acrivos, The shear-induced migration of particles in concentrated suspensions. *J. Fluid Mech.* **181**, 415–439 (1987).
13. C. J. Pipe, T. S. Majmudar, G. H. McKinley, High shear rate viscometry. *Rheol. Acta* **47**, 621–642 (2008).
14. G. D'Avino, F. Greco, P. L. Maffettone, Particle migration due to viscoelasticity of the suspending liquid and its relevance in microfluidic devices. *Annu. Rev. Fluid Mech.* **49**, 341–360 (2017).
15. P. Brunn, The motion of rigid particles in viscoelastic fluids. *J. Non-Newt. Fluid Mech.* **7**, 271–288 (1980).
16. P. C.-H. Chan, L. G. Leal, A note on the motion of a spherical particle in a general quadratic flow of a second-order fluid. *J. Fluid Mech.* **82**, 549–559 (1977).
17. M. Frank, D. Anderson, E. R. Weeks, J. F. Morris, Particle migration in pressure-driven flow of a Brownian suspension. *J. Fluid Mech.* **493**, 363–378 (2003).
18. M. Lee, M. Alcoutlabi, J. J. Magda, C. Dibble, M. J. Solomon, X. Shi, G. B. McKenna, The effect of the shear-thickening transition of model colloidal spheres on the sign of N1 and on the radial pressure profile in torsional shear flows. *J. Rheol.* **50**, 293–311 (2006).
19. K. Kang, S. S. Lee, K. Hyun, S. J. Lee, J. M. Kim, DNA-based highly tunable particle focuser. *Nat. Commun.* **4**, 2567 (2013).
20. A. M. Leshansky, A. Bransky, N. Korin, U. Dinnar, Tunable nonlinear viscoelastic "focusing" in a microfluidic device. *Phys. Rev. Lett.* **98**, 234501 (2007).
21. T. Shikata, D. S. Pearson, Viscoelastic behavior of concentrated spherical suspensions. *J. Rheol.* **38**, 601–616 (1994).
22. B. Cichocki, M. L. Ekiel-Jeżewska, E. Wajnryb, Lubrication corrections for three-particle contribution to short-time self-diffusion coefficients in colloidal dispersions. *J. Chem. Phys.* **111**, 3265–3273 (1999).
23. S. Yang, J. Y. Kim, S. J. Lee, S. S. Lee, J. M. Kim, Sheathless elasto-inertial particle focusing and continuous separation in a straight rectangular microchannel. *Lab Chip* **11**, 266–273 (2011).
24. M. M. Villone, G. D'Avino, M. A. Hulsen, F. Greco, P. L. Maffettone, Particle motion in square channel flow of a viscoelastic liquid: Migration vs. secondary flows. *J. Non-Newt. Fluid Mech.* **195**, 1–8 (2013).
25. P. Yue, J. Dooley, J. J. Feng, A general criterion for viscoelastic secondary flow in pipes of noncircular cross section. *J. Rheol.* **52**, 315–332 (2008).
26. A. Zrehen, A. Ramachandran, Demonstration of secondary currents in the pressure-driven flow of a concentrated suspension through a square conduit. *Phys. Rev. Lett.* **110**, 018306 (2013).
27. E. Nazockdast, J. F. Morris, Effect of repulsive interactions on structure and rheology of sheared colloidal dispersions. *Soft Matter* **8**, 4223–4234 (2012).
28. J. L. Trompette, M. Meireles, Ion-specific effect on the gelation kinetics of concentrated colloidal silica suspensions. *J. Colloid Interf. Sci.* **263**, 522–527 (2003).
29. S. Varchanis, Y. Dimakopoulos, C. Wagner, J. Tsamopoulos, How viscoelastic is human blood plasma? *Soft Matter* **14**, 4238–4251 (2018).
30. D. E. Smith, H. P. Babcock, S. Chu, Single-polymer dynamics in steady shear flow. *Science* **283**, 1724–1727 (1999).
31. H. A. Krebs, Chemical composition of blood plasma and serum. *Annu. Rev. Biochem.* **19**, 409–430 (1950).
32. A. Kratz, M. Ferraro, P. M. Sluss, K. B. Lewandrowski, Normal reference laboratory values. *N. Engl. J. Med.* **351**, 1548–1563 (2004).
33. T. Matsumoto, H. Inoue, Colloidal structure and properties of bovine serum globulin aqueous systems using SAXS and rheological measurements. *Chem. Phys.* **207**, 167–172 (1996).
34. S. Ikeda, K. Nishinari, Intermolecular forces in bovine serum albumin solutions exhibiting solidlike mechanical behaviors. *Biomacromolecules* **1**, 757–763 (2000).
35. V. Sharma, A. Jaishankar, Y.-C. Wang, G. H. McKinley, Rheology of globular proteins: Apparent yield stress, high shear rate viscosity and interfacial viscoelasticity of bovine serum albumin solutions. *Soft Matter* **7**, 5150–5160 (2011).
36. S. Da Vela, F. Roosen-Runge, M. W. A. Skoda, R. M. J. Jacobs, T. Seydel, H. Frielinghaus, M. Sztucki, R. Schweins, F. Zhang, F. Schreiber, Effective interactions and colloidal stability of bovine γ-globulin in solution. *J. Phys. Chem. B* **121**, 5759–5769 (2017).
37. F. Zhang, M. W. A. Skoda, R. M. J. Jacobs, R. A. Martin, C. M. Martin, F. Schreiber, Protein interactions studied by SAXS: Effect of ionic strength and protein concentration for BSA in aqueous solutions. *J. Phys. Chem. B* **111**, 251–259 (2007).
38. P. D. Godfrin, I. E. Zarraga, J. Zarzar, L. Porcar, P. Falus, N. J. Wagner, Y. Liu, Effect of hierarchical cluster formation on the viscosity of concentrated monoclonal antibody formulations studied by neutron scattering. *J. Phys. Chem. B* **120**, 278–291 (2016).
39. B. Kim, J. M. Kim, Elasto-inertial particle focusing under the viscoelastic flow of DNA solution in a square channel. *Biomicrofluidics* **10**, 024111 (2016).
40. S. O. Hong, J. M. Kim, Inertio-elastic mixing in a straight microchannel with side wells. *Appl. Phys. Lett.* **108**, 014103 (2016).
41. Y. Yurkovetsky, J. F. Morris, Particle pressure in sheared Brownian suspensions. *J. Rheol.* **52**, 141–164 (2008).
42. G. D'Avino, G. Romeo, M. M. Villone, F. Greco, P. A. Netti, P. L. Maffettone, Single line particle focusing induced by viscoelasticity of the suspending liquid: Theory, experiments and simulations to design a micropipe flow-focuser. *Lab Chip* **12**, 1638–1645 (2012).
43. F. Del Giudice, G. D'Avino, F. Greco, I. De Santo, P. A. Netti, P. L. Maffettone, Rheometry-on-a-chip: Measuring the relaxation time of a viscoelastic liquid through particle migration in microchannel flows. *Lab Chip* **15**, 783–792 (2015).
44. C. Clasen, J. P. Plog, W.-M. Kulicke, M. Owens, C. Macosko, L. E. Scriven, M. Verani, G. H. McKinley, How dilute are dilute solutions in extensional flows? *J. Rheol.* **50**, 849–881 (2006).
45. F. Del Giudice, V. Calgagno, V. E. Taliento, F. Greco, P. A. Netti, P. L. Maffettone, Relaxation time of polyelectrolyte solutions: When μ-rheometry steps in charge. *J. Rheol.* **61**, 13–21 (2017).
46. F. Del Giudice, S. J. Haward, A. Q. Shen, Relaxation time of dilute polymer solutions: A microfluidic approach. *J. Rheol.* **61**, 327–337 (2017).
47. J. Zilz, C. Schäfer, C. Wagner, R. J. Poole, M. A. Alves, A. Lindner, Serpentine channels: Micro-rheometers for fluid relaxation times. *Lab Chip* **14**, 351–358 (2014).
48. V. Tirtaatmadja, G. H. McKinley, J. J. Cooper-White, Drop formation and breakup of low viscosity elastic fluids: Effects of molecular weight and concentration. *Phys. Fluids* **18**, 043101 (2006).
49. Y. G. Liu, Y. G. Jun, V. Steinberg, Concentration dependence of the longest relaxation times of dilute and semi-dilute polymer solutions. *J. Rheol.* **53**, 1069–1085 (2009).
50. M. Rubinstein, R. H. Colby, *Polymer Physics* (Oxford Univ. Press, 2003).
51. R. H. Ewoldt, M. T. Johnston, L. M. Caretta, Experimental challenges of shear rheology: How to avoid bad data, in *Complex Fluids in Biological Systems: Experiment, Theory, and Computation*, S. E. Spagnolie, Ed. (Springer, 2015), pp. 207–241.
52. A. A. S. Bhagat, S. S. Kuntaegowdanahalli, I. Papautsky, Inertial microfluidics for continuous particle filtration and extraction. *Microfluid. Nanofluid.* **7**, 217–226 (2009).



**Acknowledgments**

**Funding:** This research was supported by the Research Program through the National Research Foundation of Korea (NRF) (nos. NRF-2016R1A2B4012328 and NRF-2018R1A5A1024127).

**Author contributions:** The project was conceived and designed by J.M.K. and B.K. J.M.K. supervised the project. B.K. performed all the experiments. B.K., S.S.L., and J.M.K. analyzed the microchannel experiments. S.Y.K., S.K., and S.-H.C. contributed to the design and analyses of the SAXS experiments. T.H.Y. contributed to the design and analyses of the particle migration experiments in the protein solutions. B.K. and J.M.K. wrote the manuscript. All authors provided helpful comments on the manuscript. **Competing interests:** The authors declare that they have no competing interests. **Data and materials availability:** All data needed to evaluate the conclusions in the paper are present in the paper and/or the Supplementary Materials. Additional data related to this work may be requested from the authors.

Submitted 20 September 2018
Accepted 29 April 2019
Published 7 June 2019
10.1126/sciadv.aav4819

**Citation:** B. Kim, S. S. Lee, T. H. Yoo, S. Kim, S. Y. Kim, S.-H. Choi, J. M. Kim, Normal stress difference–driven particle focusing in nanoparticle colloidal dispersion. *Sci. Adv.* **5**, eaav4819 (2019).


Downloaded from http://advances.sciencemag.org/ on July 17, 2019

Science Advances

# Normal stress difference–driven particle focusing in nanoparticle colloidal dispersion

Bookun Kim, Sung Sik Lee, Tae Hyeon Yoo, Sunhyung Kim, So Youn Kim, Soo-Hyung Choi and Ju Min Kim

*Sci Adv* **5** (6), eaav4819.
DOI: 10.1126/sciadv.aav4819

**ARTICLE TOOLS** http://advances.sciencemag.org/content/5/6/eaav4819

**SUPPLEMENTARY MATERIALS** http://advances.sciencemag.org/content/suppl/2019/06/03/5.6.eaav4819.DC1

**REFERENCES** This article cites 46 articles, 1 of which you can access for free
http://advances.sciencemag.org/content/5/6/eaav4819#BIBL

**PERMISSIONS** http://www.sciencemag.org/help/reprints-and-permissions

Use of this article is subject to the Terms of Service

*Science Advances* (ISSN 2375-2548) is published by the American Association for the Advancement of Science, 1200 New York Avenue NW, Washington, DC 20005. 2017 © The Authors, some rights reserved; exclusive licensee American Association for the Advancement of Science. No claim to original U.S. Government Works. The title *Science Advances* is a registered trademark of AAAS.

Downloaded from http://advances.sciencemag.org/ on July 17, 2019